Available online at www.sciencedirect.com

ScienceDirect

Procedia Structural Integrity 35 (2022) 237–246

Structural Integrity Procedia

www.elsevier.com/locate/procedia

2nd International Workshop on Plasticity, Damage and Fracture of Engineering Materials

Failure analysis of auxetic lattice structures under crush load

Kadir Günaydın[a,*], Giuseppe Sala[b], Halit S. Türkmen[c], Antonio Mattia Grande[b]

[a]*General Electric Aviation, Gebze, 41400 Kocaeli, Turkey*
[b]*Department of Aerospace Science and Technology, Politecnico di Milano, Via La Masa 34, 20156 Milano, Italy*
[c]*Aeronautics and Astronautics Faculty, Istanbul Technical University, Maslak, 34469 Istanbul, Turkey*

Abstract

Lattice structures are promising materials in the terms of energy absorption, acoustic and vibrational damping, high strength-to-weight ratios and thermal management capabilities. In particular, auxetic lattice structures, among others, show high energy absorption performances due to their characteristic negative Poisson's ratio. In this study, it is aimed to compare auxetic deformation mechanisms under quasi-static crush loads. Ti6Al4V tensile test specimens were produced with Electron Beam Melting (EBM) Additive Manufacturing (AM) technology. Moreover, a constitutive equation was derived and calibrated according to tensile results. The calibrated data were used to generate non-linear computational crush models including elastoplastic material data, damage initiation criterion, damage evaluation law and element deletion. The computational models are utilized for optimum topology design and mechanical performance prediction of different auxetic cells, including anti-tetrachiral, hexachiral, re-entrant and honeycomb lattice structures that are prone to prematurely fail under crush loading conditions. Consequently, it was found that the chiral auxetic deformation mechanism experienced better energy absorption ability over re-entrant deformation mechanism for metallic lattice structures.

Keywords: EBM; Ti6Al4V; Auxetic Lattice Structures; Crush; Ductile Damage

1. Introduction

Energy absorption structures such as sandwich structures have a crucial role in crush resisting applications including impact or blast loading. Relatively stiff face-sheets or skins and lightweight cores constitute the sandwich structures. The material and topology of the sandwich structure cores have more influence on energy absorption and load-bearing. The core material of the sandwich structures are generally formed by foam or lattices Evans et al. (2006); Lu and Yu (2003); Gunaydin and Turkmen (2019). Amongst the lattice structures, auxetic lattices come forward due to high energy absorption ability that stems from their unique ability to exhibit negative Poisson's ratio (NPR) Evans et al. (1991). In other words, opposing to conventional materials, shrinkage formation in transverse direction occurs

* Corresponding author. Tel.: +90-262-677-8410 ; fax: +90-262-677-8410.
E-mail address: kadir.gunaydin@ge.com

10.1016/j.prostr.2021.12.070

under compressive loads and lateral expansion under tensile loads Gunaydin et al. (2017). Auxetic lattice structures are generated by tailoring the geometrical parameters to obtain negative Poisson's ratio, and they are also classified as meta-materials due to their unique properties.

Besides the large global flexibility and large local deformation within elastic limits, auxetic materials exhibit improved mechanical properties. The superiority of auxetic structures over conventional materials are summarized as follows: (a) improved edgewise (in-plane) indentation resistance, (b) high fracture toughness, (c) better transverse shear modulus Wu et al. (2019); Gunaydin et al. (2019). Auxetic structures have been utilized in different applications; exemplifying, innovative stent designs Wu et al. (2018); Ruan etal. (2018), smart actuators, propellers, flexible microelectronics, and biomechanical devices Wu et al. (2018); Ma et al. (2018). Numerous studies on NPR structures are found in the literature; however, the first NPR material was developed by Lakes (1987) as in the form of artificial synthetic foam material, and the term of "*auxetic*" was first asserted and used by Evans et al. (1991). Three different well-known auxetic deformation mechanisms are prevalent; rotating rigid, re-entrant and chiral. Rotating rigid auxetics do not find a place in energy absorption fields due to their highly rigid deformation mechanism. Re-entrant auxetic structures are obtained by altering the cell wall angles of the honeycomb hexagonal lattice structures. Chiral structures are formed by the interconnection of cell walls (ligaments) and cylindrical nodes. Auxetic lattice structures are divided into two groups in dimensional levels: 2D and 3D. For the 2D auxetic lattice structures, the in-plane direction shows the orientation in which the auxetic structure experiences NPR Gunaydin et al. (2021). Out-of-plane direction is the opposite. NPR is experienced under elastic deformation.

Numerous researchers proposed elastic constitutive equations for various NPR lattices Chen et al. (2013); Assidi and Ganghoffer (2012); Gonella and Ruzzene (2008); Bacigalupo and De Bellis (2015); Huang et al. (2017); Laroto et al. (2010) and zero Poisson's ratio (ZPR) Lira et al. (2011). For example, Chen et al. (2013) offered the elastic constitutive equations of anti-tetrachiral lattices and validated equations with experimental results. Li et al. (2017) and Wu et al. (2017) proposed new tetrachiral and anti-tetrachiral auxetic lattice designs with their analytical expressions for in-plane mechanical properties and varified the expression with experimental and FEA results. Moreover, topology parameters directly affect NPR behaviours. Such as the ratio of ligament length to node radius for anti-trichiral is to be less than 5.5 for the exhibition of auxeticity Hu et al. (2009, 2019). In addition to elastic studies, the studies on the effect of large deformation and topology parameter were performed for different NPR lattice. Zhou et al. (2017) studied the large compressive deformation of re-entrant lattices in the in-plane direction. Zhang et al. (2015) performed a study to measure the effect of different cell angles and different strain rates of re-entrant honeycombs under impact loads. Ingrole et al. (2017) produced 3D modified auxetic re-entrant lattice cells to examine the in-plane crushing behaviour and suggested modified re-entrant lattice structures as promising candidate for energy absorption. Zhou et al. (2017) studied compressive behaviour of 3D printed metal re-entrant lattice structure using different topology parameters. Dong et al. (2019) studied the effect of wall thickness on the deformation mode and auxeticity.

In this study, the failure analysis of re-entrant, anti-tetrachiral and hexachrial (chiral) lattices exhibiting NPR and honeycomb lattice structure were investigated under compressive quasi-static loading in-plane direction in order to investigate the effect of failure and deformation modes for four different lattice structures having different deformation mechanisms. To the authors' knowledge, no other failure and energy absorption comparison analyses of re-entrant, honeycomb, anti-tetrachiral and hexachiral lattice structures have been addressed in the literature. For the material input for the analysis, EBM printed Ti6Al4V tensile test results were used to calibrate a material data for the simulation of the elastoplastic material behaviour and failure. As to the failure analysis classical metal plasticity is used in conjunction with ductile damage initiation criterion and progressive damage evolution law for ductile metals. As a result, two different auxetic deformation mechanism and regular honeycomb deformation are compared.

2. Lattice Structures

Three different auxetic deformation mechanism is well-known for lattice structures, rotating rigid, re-entrant and anti-tetrachiral Kelkar et al. (2020). Rotating rigid auxetic structures are not proper lattice structures for energy absorption applications by cause of involving bulky structures. Thus, the chiral and re-entrant deformation mechanism is the topic of study. Due to similar outbox geometries, anti-tetrachiral, hexachiral, regular honeycomb and re-entrant lattice structures were utilized in this study for failure analysis to investigate deformation mechanisms Gunaydin et

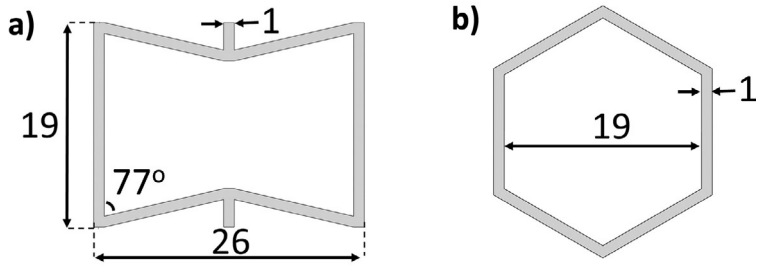

Fig. 1. Dimensions of (a) re-entrant auxetic and (b) honeycomb lattice structure (all dimensions are in mm).

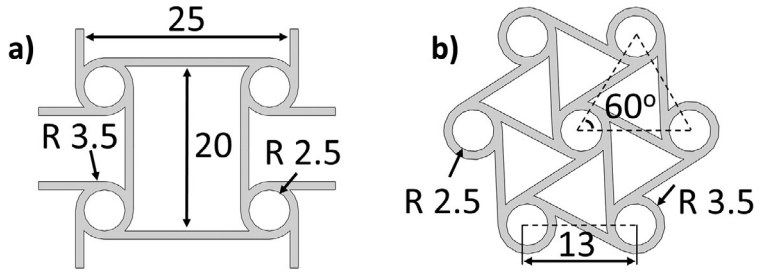

Fig. 2. Dimensions of (a) anti-tetrachiral and (b) hexachiral auxetic lattice structure (all dimensions are in mm).

al. (2019). Moreover, lattice structures are formed by the interconnection of repeated cells, called unit cells. Any topological change in unit cells changes the response of the structure.

2.1. *Re-entrant and honeycomb lattice structures*

Re-entrant auxetic structures are obtained by altering the cell wall angles of the regular honeycomb hexagonal lattice structures. The unit cell deformation mechanism of the re-entrant structures is formed by the rotation of the diagonal ligaments Gunaydin et al. (2019). On contrary to chiral auxetic structures, re-entrant auxetic structures are generated by only using ligaments. The direct connection of ligaments with defined angles creates auxeticity. Thus, the production of re-entrant auxetic structures provides easiness due to its regular shaped ligament based structure. Dimensions of the re-entrant auxetic and honeycomb structure are seen in Fig. 1.

2.2. *Anti-tetrachiral and tetrachiral lattice structures*

The chiral auxetic structures are formed by the interconnected nodes and ligaments and each ligament is connected to nodes tangentially. The number of the ligaments characterises the type of chiral structure. Such as, hexachiral, tetrachiral and trichiral lattices which consist of 6, 4, and 3 ligaments that are connected to each node, respectively. The term ”*prefix*” is utilized for the characterization of ligament and node connection, and in this configuration, ligaments are connected on the opposite sides of the nodes. Moreover, all the chiral lattice structures do not exhibit auxeticity, only chiral lattice structures having 6 and 4 ligaments connected to one node and anti-trichiral system with short ligaments exhibit NPR Bacigalupo and De Bellis (2015). For this reason, dimensions of lattice structures are benefited from the study of Johnston and Kazanci Johnston and Kazanci (2021). Dimensions of the anti-tetrachiral and hexachiral auxetic structure are shown in Fig. 2. The dimensions of the re-entrant, anti-tetrachiral and hexachiral structures were captured from the literature to be granted the auxeticity. The dimension of the regular honeycomb is defined in terms of equal outbox dimension and ligament thickness.

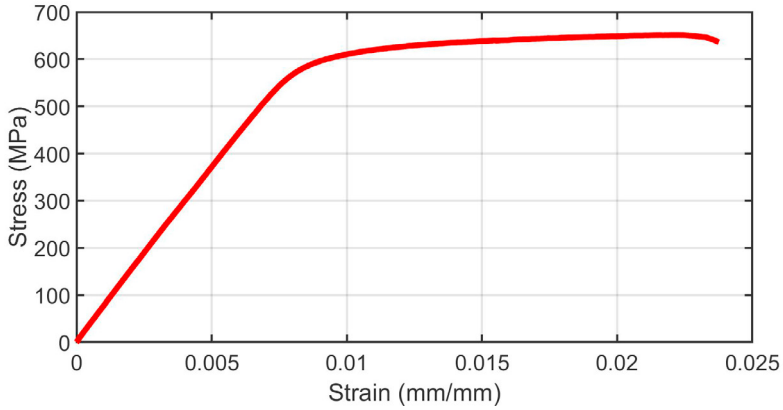

Fig. 3. Engineering stress-strain graph for EBM printed Ti6Al4V.

3. Material Characterization

EBM is a powder bed fusion technology in which an electromagnetically displaced and focused electron beam is used to selectively melt a thin layer of metal powder Körner (2009). The process operates in a high vacuum atmosphere, which reduces contamination and oxidation issues compared with other AM processes. The electron beam itself is used to pre-heat every layer to a target temperature before melting the powder, with the consequent effect of considerably reducing thermal stresses in the part. The high ambient temperature in the build chamber also prevents the formation of α' martensitic brittle phase Edwards et al. (2013). Thus, it is convenient to use EBM printed parts asbuilt. To understand the mechanical behaviour and characterize EBM printed parts tensile tests are conducted according to ASTM E8M standard. According to the tensile test result, a constitutive equation is formed and used after the selection and calibration process to verify the numerical model for optimum topology design and mechanical performance forecast using a non-linear computational model with failure analysis.

Table 1. Damage initiation and evolution parameters for EBM printed Ti6Al4V.

Fracture Strain	Stress Triaxiality	Strain Rate	Displacement at Failure
0.021	1/3	0	0.001

First of all, damage initiation parameters are needed to extract from tensile test results for failure simulation. For this reason, the required material data of fracture strain and stress triaxiality is extracted from the true stress-strain curve. In addition, the strain rate of the tensile test is needed as an input. However, if the material is strain independent or the strain rate of the material characterization test and analysis strain rate is equal, then the parameter is set as zero. The fracture strain is the strain point on the stress-strain curve when the corresponding ultimate stress is reached. Strain triaxiality is defined as the ratio of hydrostatic pressure stress to von Mises equivalent stress. In the uniaxial tensile tests, it is accepted that there is no transverse strain and shear stresses due to the single load execution and its direction. Thus, stress triaxiality is always equal to 1/3 when the tensile test data is used. As a next step, damage evolution parameters are needed, and it is based on the total energy that is utilized in the necking region. The needed fracture energy is calculated for a single FEM element according to its characteristic element length. Therefore, all the mesh elements are provided to be equal in size. Characteristic element lengths are equal to the ratio of the element volume to its largest surface area, and half of this value is used for quadratic elements. Finally, displacement at failure value is calculated using the ratio of fracture energy to ultimate stress Abaqus User Manual (2020). In the Table 1, damage initiation and evolution values are exhibited.

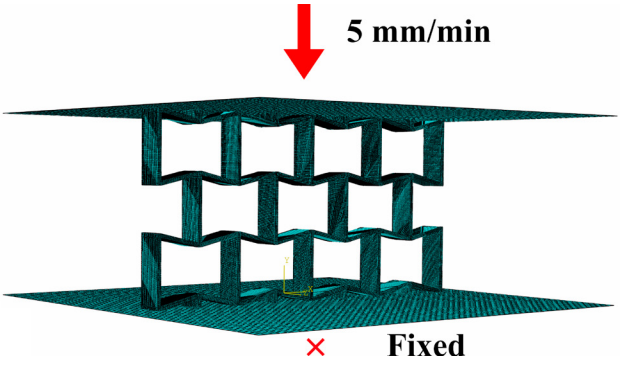

Fig. 4. Meshed re-entrant lattice structure and boundary conditions.

4. Numerical Analysis

As for the numerical analysis of the crush of lattice structures, explicit finite element analyses are performed by using the Simulia/Abaqus Explicit finite element software. The choice of element type and size plays a vital role to obtain accurate results while minimising the computational cost. So that the C3D8I eight-node linear brick element is selected, and convergence studies have been conducted. C3D8I eight-node linear brick elements are improved by incompatible modes to enhance the capturing of bending behaviour. Because of the complex shape and curved edges, in the meshing processes, a relatively irregular mesh is obtained in some regions; however, the uniform mesh is provided in the critic regions. In addition to the linear elasticity material model, for the simulation of the plastic behaviour and failure, classical metal plasticity material is used in conjunction with ductile damage initiation criterion and progressive damage evolution law for ductile metals. General contact interaction with the penalty algorithm is prescribed among all the surfaces of the structures. Discretized re-entrant auxetic lattice structure and its boundary conditions are shown in Fig. 4.

5. Results

The load-deflection curve of crush structures can be divided into three parts called elastic, plateau and densification phases. Most of the energy is absorbed by plastic deformation and fractures, and a lower amount of energy can be absorbed by elastic deformation. Therefore, an elongated plateau phase is necessary for improved energy absorption. The densification phase also can be directly observed in the load-deflection graphs as a dramatic and continuous increase in the load. The onset of the densification phase is an important variable that is taken into the account for energy-absorption indexes calculations. The peak loads in which the plateau phase start and densification points are shown in Fig. 5. The peak point was reached earlier within the honeycomb and anti-tetrachiral structures and densification points of hexachiral and anti-tetrachiral are nearly on the same displacement values. However, re-entrant structure reached densification point earlier and honeycomb has the latest onset of densification point. In addition to initial peak loads, second peak loads emerged due to the deformation pattern of the structures. Such as, the nodes of the hexachiral structures aligned and touched each other in the loading direction, thus high peak load occured until the failure of the nodes. Moreover, hexachiral and anti-tetrachiral exhibited longer plateau regions and higher loads in the region in comparison to re-entrant and honeycomb. However, an erratic curve is monitored in the plateau region for anti-tetrachiral and hexachiral structure due to continuous failures and increasing ligaments interactions. For better comparison, the calculation of total energy absorption is required. The energy absorption (EA) is described as the area under the load-deflection curve and can be calculated using Equation 1.

$$EA = \int_0^d F d\delta \tag{1}$$

In Equation 1, d is the maximum deflection until the onset of the densification phase, and F is the reaction force. The mass of the crushed structure is also important to have better energy absorption performance with less mass, and energy absorption capability can be measured with specific energy absorption (SEA) value as shown in Equation 2.

$$SEA = \frac{EA}{m} \tag{2}$$

The calculated EA values for re-entrant, honeycomb, anti-tetrachiral and hexachrial structures are 41.05, 34.28, 11084 and 119.19 J, respectively. As to SEA values, re-entrant, honeycomb, anti-tetrachiral and hexachrial lattice structures exhibited 1.84, 1.63, 3.37 and 2.26 kJ/kg, respectively. In comparison to both EA and SEA values, structures having chiral deformation mechanism presented better energy absorption performance. The differences in EA and SEA values can be expressed by investigating the deformation of both structures, as seen in Fig. A.6 and B.7. The relative density of the hexachiral is the highest with a value of 1380 kg/m^3 and it is followed by anti-tetrachiral with a value of 869 kg/m^3. The increase in density also rises the total absorbed energy Gibson and Ashby (1999); however, it decreases SEA value. Thus, SEA value is a better index for energy absorption ability comparison. Furthermore, the deformation mechanism involving wrapping ligaments over nodes increases the material agglomeration under the crush zone as shown in the anti-tetrachiral and hexachiral structures. This material agglomeration increases with the displacement gradually. However, the deformation pattern in the re-entrant and honeycomb structures are not homogeneous as anti-tetrachiral, and also less failure is observed during the crush which decreases the pikes in the load-displacement curves. Thus, the chiral deformation mechanism absorbs more energy. Furthermore, anti-tetrachiral and re-entrant lattice structures for defined geometrical parameters showed auxeticity, lateral shrinkage explicitly seen in Fig. A.6 and B.7.

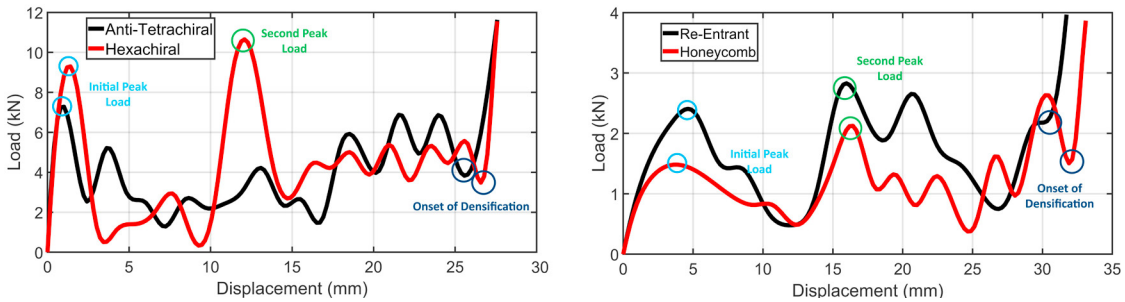

Fig. 5. Load - displacement curves for anti-tetrachical, hexachiral, re-entrant and honeycomb lattice structures.

6. Conclusion

The material characterization and calibration of EBM printed Ti6Al4V is performed to obtain elastoplastic constitutive equation, damage initiation criterion and damage evaluation law parameters in order to simulate crush behaviour of re-entrant, honeycomb, anti-tetrachiral and hexachiral lattice structures. Moreover, deformation modes are evaluated for both structures to elucidate the deformation mechanism effect on energy absorption. According to the energy absorption results, the anti-tetrachiral and hexachiral lattice structure absorbs almost three times more than the re-entrant and honeycomb lattice structure. Furthermore, the specific energy absorption value for the anti-tetrachiral structure is two times more than the re-entrant and honeycomb lattice structure and greater than the hexachiral structure. Re-entrant and honeycomb structures nearly exhibit similar EA and SEA values. All auxetic structures except hexachiral showed auxeticity during the crush for the defined dimensions. Hexachiral did not experience auxiticity due to brittle material and high relative density. Erratic curve is monitored in the plateau region for anti-tetrachiral and hexachiral structure due to continuous failures and increasing ligaments interactions. However, re-entrant structure is experienced smooth curve in the plateau region due to higher inner gaps and longer ligaments. For further research, experimental validation study is required.

Acknowledgements

This study is supported by Technological and Scientific Council of Turkey (TUBITAK) under Technology and Innovation Support Program (Grant Number: 5158001).

Appendix A. Deformation patterns of re-entrant and honeycomb lattice structures

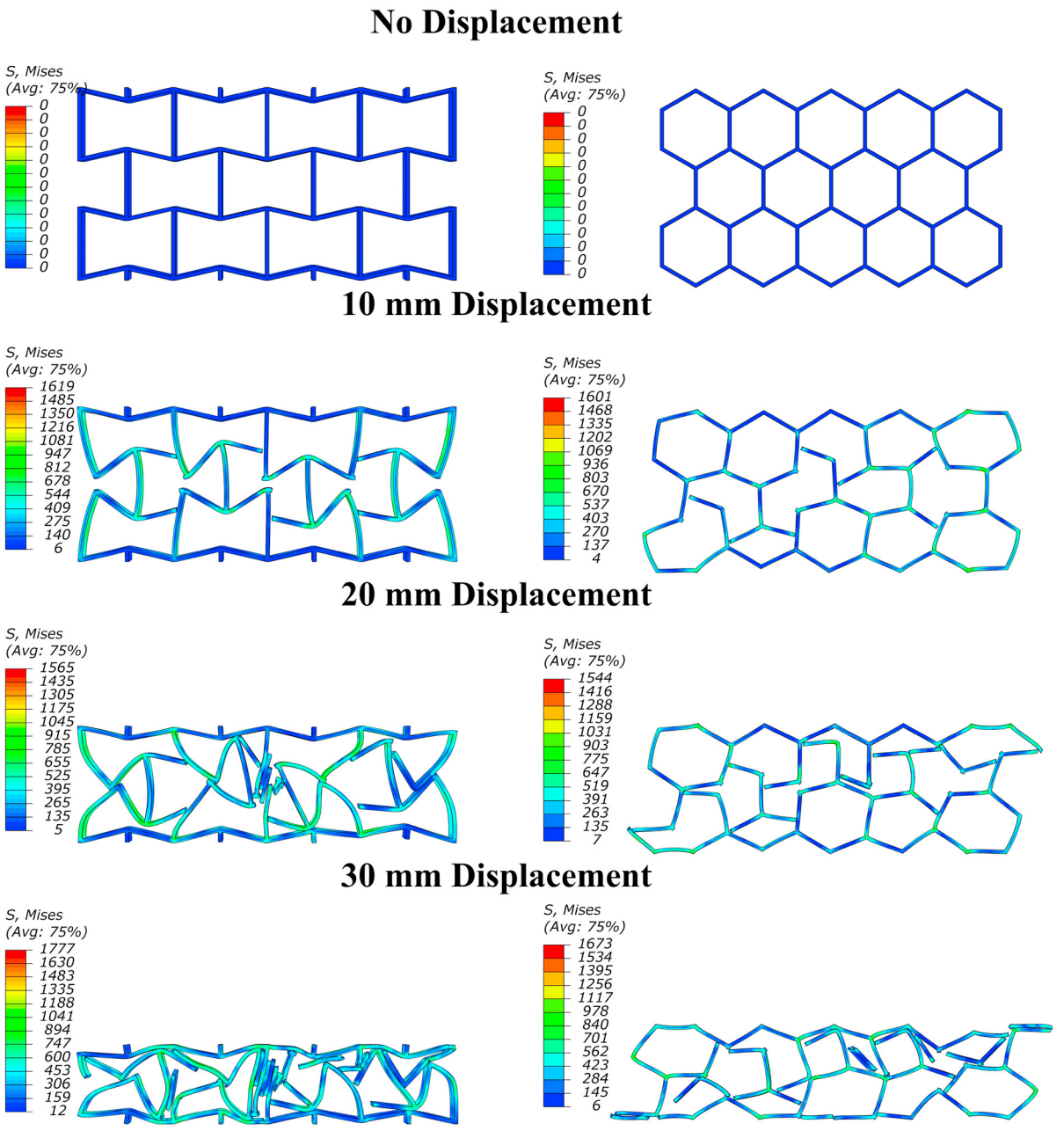

Fig. A.6. Deformation patterns of re-entrant and honeycomb lattice structures with 10 mm interval.

Appendix B. Deformation patterns of anti-tetrachiral and hexachrial lattice structures

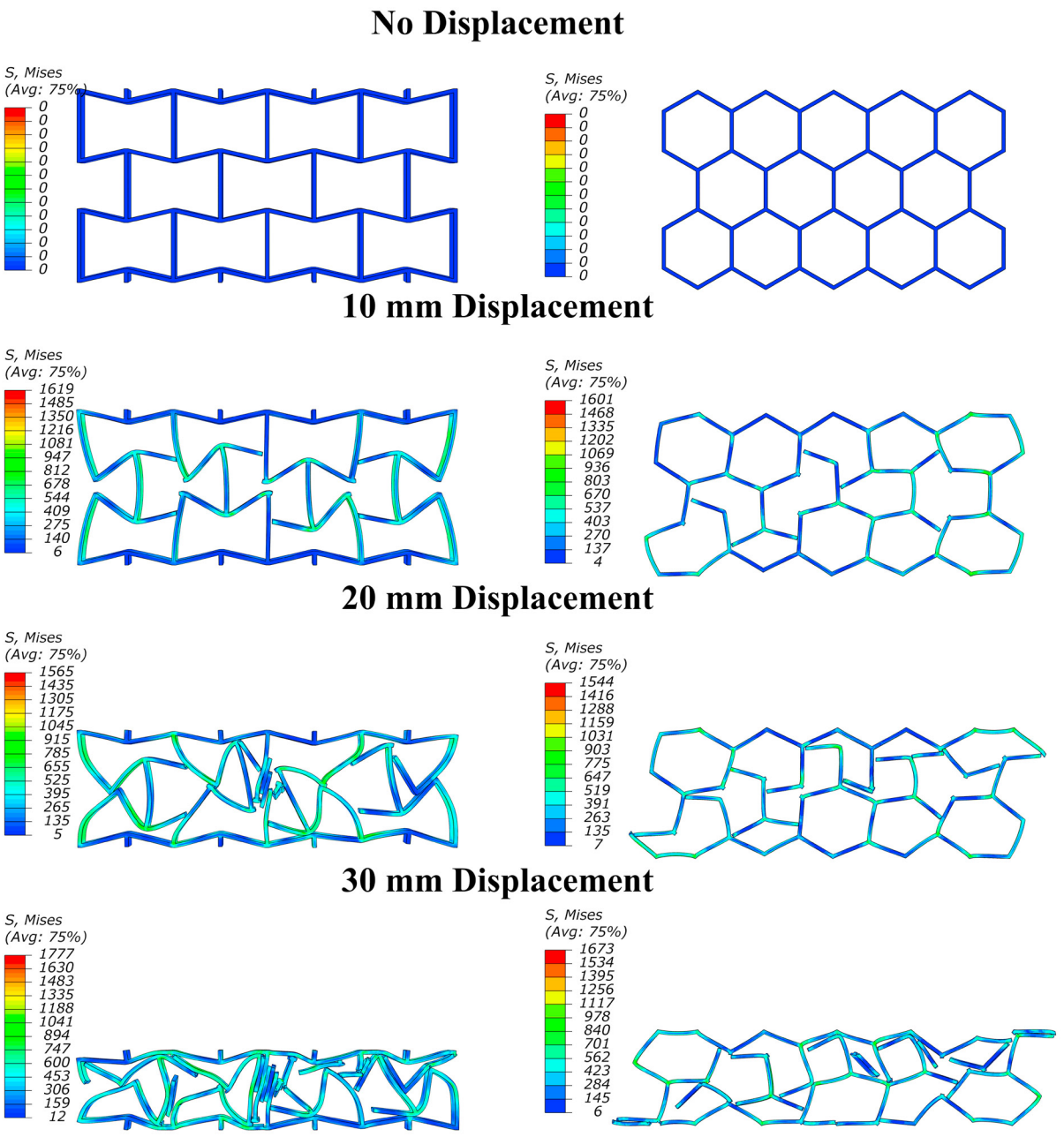

Fig. B.7. Deformation patterns of anti-tetrachiral and hexachrial lattice structures with 10 mm interval.

References

Lu, G., Yu, T., 2003. Energy Absorption of Structures and Materials, in "*In Woodhead Publishing Series in Metals and Surface Engineering*". Woodhead Publishing, pp. 144-173.

Evans, A. G., Hutchinson, J. W., Fleck, Norman A., Ashby, M. F., Wadley, H. N. G., 2001. The Topological Design of Multifunctional Cellular Metals. Progress in Materials Science 46, 309–327.

Evans, K. E., Nkansah, M. A., Hutchinson, I. J., Rogers, S. C., 1991. Molecular Network Design. Nature 353, 124–124.

Gunaydin, K., Eren, Z., Scarpa, F., 2017. "Experimental Investigation of Auxetic Structures Subjected to Quasi Static Axial Load," 2017 8th International Conference on Recent Advances in Space Technologies (RAST). Istanbul, Turkey, 7–10.

Gunaydin, K., Eren, Z., Kazanci, Z., Scarpa, F., Grande, A. M., Turkmen, H. S., 2019. In-plane Compression Behavior of Anti-tetrachiral and Re-entrant Lattices. Smart Materials and Structures 28, 115028.

Gunaydin K., Turkmen H. S., 2019. "In-Plane Quasi-Static Crushing Finite Element Analysis of Auxetic Lattices," 2019 9th International Conference on Recent Advances in Space Technologies (RAST). Istanbul, Turkey, 645–648.

Wu, W., Qi, D., Liao, H., Qian, G., Geng, L., Niu, Y., Liang, J., 2018. Deformation Mechanism of Innovative 3D Chiral Netamaterials. Scientific Reports 8, 1–10.

Wu, We., Hu, W., Qian, G., Liao, H., Xu, X., Berto, F., 2019. Mechanical Design and Multifunctional applications of Chiral Mechanical Metamaterials: A Review. Materials & Design 180, 107950.

Ruan, X. L., Li, J. J., Song, X. K., Zhou, H. J., Yuan, W. X., Wu, W. W., Xia, R., 2018. General Relationship for the Thermal Oxidation of Silicon. International Journal of Applied Mechanics 10, 1850105.

Wu, W., Geng, L., Niu, Y., Qi, D., Cui, X., Fang, D., 2018. Mechanical Design ofAntichiral-Reentrant Hybrid Intravascular Stent. Extreme Mechanics Letters 20, 104–111.

Ma, C., Lei, H., Liang, J., Wu, W., Wang, T., Fang, D., 2018. Macroscopic Mechanical Response of Chiral-Type Cylindrical Metastructures Under Axial Compression Loading. Materials & Design 158, 198–212.

Lakes, R., 1987. Foam Structures with A Negative Poisson's Ratio. American Association for the Advancement of Science 235, 1038–1041.

Zhou, Z., Zhou, J., Fan, H., 2017. Plastic Analyses of Thin-Walled Steel Honeycombs with Re-entrant Deformation Style. Materials Science and Engineering: A 688, 123–133.

Chen, Y. J., Scarpa, F., Liu, Y. J., Leng, J. S., 2013. Elasticity of Anti-Tetrachiral Anisotropic Lattices. International Journal of Solids and Structures 50, 996–1004.

Assidi, M., and Ganghoffer, J., 2012. Composites with Auxetic Inclusions Showing Both An Auxetic Behavior and Enhancement of Their Mechanical Properties. Composite Structures 94, 2373–2382.

Gonella, S., Ruzzene, M., 2008. Homogenization and Equivalent In-Plane Properties of Two-Dimensional Periodic Lattices. International Journal of Solids and Structures 45, 2897–2915.

Bacigalupo, A. and De Bellis, M. L., 2015. Auxetic Anti-Tetrachiral Materials: Equivalent Elastic Properties and Frequency Band-Gaps. Composite Structures 131, 530–544.

Huang, J., Zhang, Q., Scarpa, F., Liu, Y., Leng, J., 2017. In-Plane Elasticity of A Novel Auxetic Honeycomb Design. Composites Part B: Engineering 110, 72–82.

Lorato, A., Innocenti, P., Scarpa, F., Alderson, A., Alderson, K. L., Zied, K. M., Ravirala, N., Miller, W., Smith, C. W., Evans, K. E., 2010. The Transverse Elastic Properties of Chiral Honeycomb. Composites Science and Technology 70, 1057–1063.

Lira, C., Scarpa, F., Tai, Y. H., Yates, J. R., 2011. Transverse Shear Modulus of SILICOMB Cellular Structures. Composites Science and Technology 71, 1236–1241.

Gunaydin, K., Tamer, A., Turkmen, H. S., Sala, G., Grande, A. M., 2021. Chiral-Lattice-Filled Composite Tubes under Uniaxial and Lateral Quasi-Static Load: Experimental Studies. Applied Sciences 11, 3735.

Li, H., Ma, Y., Wen, W., Wu, W., Lei, H., Fang, D., 2017. In Plane Mechanical Properties of Tetrachiral and Antitetrachiral Hybrid Metastructures. Journal of Applied Mechanics 84,8.

Wu, W., Tao, Y., Xia, Y., Chen, J., Lei, H., Sun, L., Fang, D., 2017. Mechanical Properties of Hierarchical Anti-Tetrachiral Metastructures. Extreme Mechanics Letters 16, 18–32.

Hu, L. L., Wu, Z. J., Fu, M. H., 2009. Mechanical Behavior of Anti-Trichiral Honeycombs Under Lateral Crushing. International Journal of Mechanical Sciences 140, 537–546.

Hu, L. L., Luo, Z. R., Zhang, Z. Y., Lian, M. K., Huang, L. S., 2019. Mechanical Property of Re-entrant Anti-Trichiral Honeycombs Under Large Deformation. Composites Part B: Engineering 163, 107–120.

Zhang, X., Ding, H., An, L., Wang, X., 2015. Numerical Investigation on Dynamic Crushing Behavior of Auxetic Honeycombs with Various Cell-Wall Angles. Advances in Mechanical Engineering 7, 679678.

Ingrole, A., Hao, A., Liang, R., 2017. Design and Modeling of Auxetic and Hybrid Honeycomb Structures for In-Plane Property Enhancement. Materials & Design 117, 72–83.

Dong, Z., Li, Y. Zhao, T., Wu, W., Xiao, D., Liang, J., 2019. Experimental and Numerical Studies on The Compressive Mechanical Properties of The Metallic Auxetic Reentrant Honeycomb. Materials & Design 182, 108036.

Wu, W., Song, X., Liang, J., Xia, R., Qian, G., Fang, D., 2018. Mechanical Properties of Anti-Tetrachiral Auxetic Stents. Composite Structures 185, 381–392.

ABAQUS User Manual, 2020.

Gibson, L. J., Ashby, M. F., 1999. Cellular Solids: Structure and Properties. Cambridge University Press.

Körner, C., 2009. Additive Mnufacturing of Metallic Components by Selective Electron Beam Melting—A Review. International Materials Reviews

61, 361–377.
Edwards, P., O'conner, A., Ramulu, M., 2013. Electron Beam Additive Manufacturing of Titanium Components: Properties and Performance. Journal of Manufacturing Science and Engineering 135, 061016.
Kelkar, P. U., Kim, H. S., Cho, K., Kwak, J. Y., Kang, C., Song, H., 2020. Cellular Auxetic Structures for Mechanical Metamaterials: A Review. Sensors 20, 3132.
Johnston, R., Kazanci, Z., 2021. Analysis of Additively Manufactured (3D printed) Dual-Material Auxetic Structures Under Compression. Additive Manufacturin 38, 101783.